HI Content of Group Galaxies from the FAST All Sky HI Survey

SHULAN YAN (鄢淑澜) , ANDREW MA, QINGZHENG YU (余清正) , TAOTAO FANG (方陶陶) , CHUAN HE (何川) , AND MING ZHU (朱明) , TAOTAO FANG (方陶陶) , AND MING ZHU (朱明) , TAOTAO FANG (方陶陶)

¹Department of Astronomy, Xiamen University, Xiamen, Fujian 361005, People's Republic of China
 ²International School of Beijing, 10 An Hua Street, Shunyi District, Beijing 101318, People's Republic of China
 ³Dipartimento di Fisica e Astronomia, Università degli Studi di Firenze, Via G. Sansone 1, 50019 Sesto Fiorentino, Firenze, Italy
 ⁴INAF - Osservatorio Astrofisico di Arcetri, Largo E. Fermi 5, I-50125 Firenze, Italy
 ⁵National Astronomical Observatories, Chinese Academy of Sciences (NAOC), Beijing 100101, People's Republic of China
 ⁶Guizhou Radio Astronomical Observatory, Guiyang 550025, People's Republic of China
 ⁷Guizhou Provincial Key Laboratory of Medium and Low Frequency Radio Astronomy Technology and Application, Guiyang 550025, People's Republic of China

ABSTRACT

We investigate the atomic gas (H I) content of galaxies in groups using early data from the FAST All Sky H I survey (FASHI). Taking advantage of FAST's blind, wide-area coverage and uniform sensitivity, we assemble a sample of 230 group galaxies and a matched control sample of isolated systems, and apply censored-data modeling to include both detections and non-detections. At fixed stellar mass and color, we find that the global median H I fraction of group galaxies differs from that of controls by only -0.04 dex (95% CI [-0.18, 0.16]), indicating at most a mild average offset. The signal is not uniform across populations: satellites are H I-poor (median $\Delta f_{\rm HI} = -0.12$ dex), whereas centrals are consistent with normal to mildly H I-rich (median $\Delta f_{\rm HI} = 0.13$ dex). Group galaxies located within $0.5R_{180}$ and in denser systems (richness > 10 or local density $\Sigma > 10$ gal Mpc⁻²) show stronger negative offsets, whereas galaxies in the outskirts are statistically indistinguishable from the controls. These results refine earlier reports of global group H I deficiency: with deeper blind data and uniform treatment of upper limits, we show that H I depletion is primarily confined to satellites and compact cores rather than being ubiquitous across groups.

Keywords: Galaxy evolution (594) — Galaxy groups (597) — Interstellar atomic gas (833)

1. INTRODUCTION

Galaxy groups and clusters serve as key laboratories for studying how environmental conditions shape galaxy evolution. Mechanisms such as ram pressure stripping, tidal interactions, and strangulation can suppress star formation and deplete the cold gas reservoirs of galaxies in groups (Gunn & Gott 1972; Cayatte et al. 1990; Vollmer et al. 2001; Chung et al. 2009; Cortese et al. 2021; Moretti et al. 2023; Luber et al. 2025). Atomic hydrogen (HI), a major component of the interstellar medium, often extends well beyond the stellar disk,

Corresponding author: Qingzheng Yu

qingzheng.yu@unifi.it

Corresponding author: Taotao Fang

fangt@xmu.edu.cn

making it a sensitive tracer of environmental processes and the neutral gas content in galaxies (Cayatte et al. 1994; Hibbard & van Gorkom 1996; Serra et al. 2012). Previous studies have reported significant H I deficiencies in galaxy groups and clusters (Huchtmeier 1997; Verdes-Montenegro et al. 2001; Williams et al. 2002; Cortese et al. 2011; For et al. 2021). Among the various mechanisms, ram pressure stripping is frequently invoked to explain both the rapid removal of gas and the pronounced H I deficiencies observed in dense environments (Boselli & Gavazzi 2006; Chung et al. 2009; Jaffé et al. 2015; Stark et al. 2016; Ai & Zhu 2018; Brown et al. 2023).

Recent H_I observations of HCGs with VLA and MeerKAT have revealed widespread H_I deficiencies, particularly in systems exhibiting extended H_I structures (Jones et al. 2023; Sorgho et al. 2025). For et al. (2021) also reported that nearly half ($\sim 46.5\%$) of the galaxies in the Eridanus group are H I deficient. H I depletion is more pronounced in galaxies residing in denser environments or located closer to cluster centers (Solanes et al. 2001; Odekon et al. 2016; Hu et al. 2021; Deb et al. 2023). In contrast, some processes can replenish or sustain gas reservoirs. For example, gas-rich minor mergers may increase the gas content of clusters and thereby enhance star formation activity (Janowiecki et al. 2017). Some group galaxies with low H I content exhibit enhanced molecular gas reservoirs and continue to form stars, in some cases within stripped gas tails (Moretti et al. 2020; Zabel et al. 2022; Moretti et al. 2023).

Target H_I observations provide detailed information on the gas properties of galaxies in groups, but these studies are often limited by small sample sizes and by the challenge of constructing suitable control samples from the same data. Interferometric observations offer high spatial resolution, but they may miss diffuse or extended HI, thereby exaggerating the deficiency in evolved groups. To address these limitations, several studies have employed blind HI surveys to establish scaling relations and to investigate the gas content of group galaxies (Dénes et al. 2014; Catinella et al. 2018; Zu 2020; For et al. 2021; Li et al. 2022). HI scaling relations vary in different works, relying on diverse galaxy properties they employed, such as optical magnitude, color, stellar mass, halo mass, or morphology (Catinella et al. 2010; Jones et al. 2018; Zu 2020; For et al. 2021; Lu et al. 2024). The heterogeneous scaling relations of HI content can also shift deficiency numerically. Most previous analyses have concentrated on HI-detected galaxies or treated non-detections in a simplified way, potentially introducing bias. A comprehensive assessment requires incorporating upper limits and applying censored-data modeling techniques.

The Five-hundred-meter Aperture Spherical radio Telescope (FAST) is a powerful single-dish telescope. The FAST all sky H I survey (FASHI) project is expected to detect over 100,000 extragalactic H I sources covering the sky in -14° < decl. < $+66^{\circ}$ up to $z \sim 0.35$ (Zhang et al. 2024). FASHI enables the study of extragalactic H I across previously unexplored regions of the sky. Because the same data cubes cover both group cores and their surrounding environments, consistent selection functions can be applied to groups and control galaxies. Uniform, noise-based upper limits derived from the rms maps provide position-dependent sensitivity estimates, allowing censored likelihoods without simplified impu-

tation. FASHI has a frequency range of 1.0-1.5 GHz, achieving a detection sensitivity of ~ 0.76 mJy beam⁻¹ at a velocity resolution of 6.4 km s⁻¹ (Jiang et al. 2019, 2020). More specifically, FASHI is capable of detecting H I sources down to $M_{\rm HI} \sim 10^9 M_{\odot}$ with a signal-to-noise ratio of 10 and a velocity width of $W_{50}=200$ km s⁻¹ at $z\sim 0.03$. This performance represents a significant improvement over HIPASS, ALFALFA and WALLABY (Barnes et al. 2001; Haynes et al. 2018; Koribalski et al. 2020). The sensitivity of FASHI makes it possible to detect faint and diffuse H I gas that is often missed by interferometric observations (Zhu et al. 2021; Liu et al. 2023; Xu et al. 2023; Yu et al. 2023; Zhou et al. 2023), offering a clear advantage for probing stripped H I in group environments.

To better understand H I deficiency in galaxy groups, we cross-match the FASHI data with SDSS DR7 group catalog from Yang et al. (2007). We selected galaxies based on their optical properties to avoid selection biases toward H I detections. We also consider galaxies without H I detections to establish a robust scaling relation, thereby enabling a statistically robust investigation of atomic gas in galaxy groups.

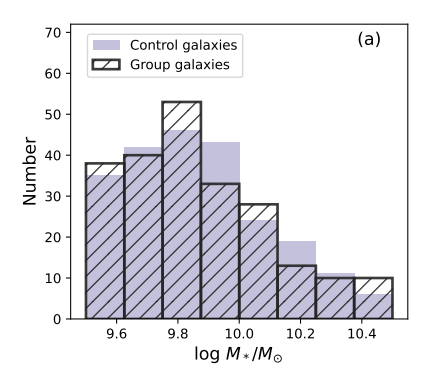
This paper is structured as follows. In Section 2, we describe the sample selection of galaxies in groups and isolated galaxies as the control sample. Section 3 presents our main results on H I gas in group galaxies. Section 4 provides further discussion of these findings, and Section 5 summarizes the main results. Throughout this paper, we adopt the standard Λ -CDM cosmology with $\Omega_m = 0.3$, $\Omega_{\Lambda} = 0.7$, $H_0 = 70$ km s⁻¹Mpc⁻¹ and $h = H_0/(100 \text{ km s}^{-1}\text{Mpc}^{-1})$.

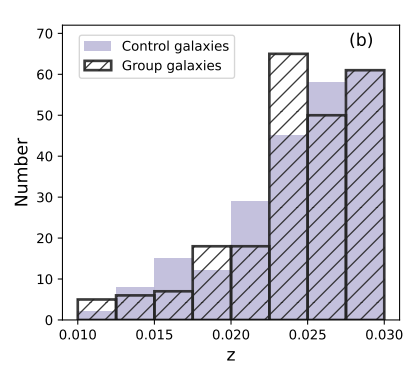
2. METHOD

2.1. Optical and HI Data

We adopt the group catalog from Yang et al. (2007) 8 , constructed with a halo-based group finder applied to SDSS galaxies (Yang et al. 2005). This catalog includes 472, 416 groups within the redshift range $0.01 \le z \le 0.2$, of which 68, 170 have at least two member galaxies. We identify the brightest galaxy in each group as the central, while the others are classified as satellites. Stellar mass and star formation rate (SFR) are taken from the GALEX-SDSS-WISE Legacy Catalog (GSWLC; Salim et al. (2016)), derived through UV-optical spec-

⁸ https://gax.sjtu.edu.cn/data/Group.html





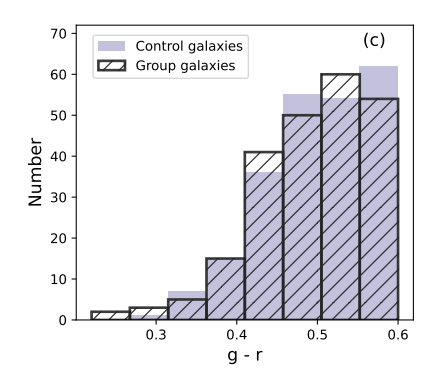


Figure 1. Distributions of basic properties for isolated galaxies (purple) and group galaxies (black). Panel (a), (b), and (c) correspond to stellar mass, redshift, and color g-r, respectively.

tral energy distribution fitting.

We use the extragalactic H I data from the FASHI project (Zhang et al. 2024). The first data release of the FASHI project covers the sky regions $0^{\rm h} \leq {\rm RA} \leq 17.3^{\rm h}$, $22^{\rm h} \leq {\rm RA} \leq 24^{\rm h}$ and $-6^{\circ} \leq {\rm DEC} \leq 0^{\circ}$, $30^{\circ} \leq {\rm DEC} \leq 66^{\circ}$. In total, FASHI has detected 41,741 extragalactic H I sources at z < 0.09. More than 94% have a signal-to-noise ratio (SNR) above 10. The beam size of FAST is $\sim 2'.9$ at 1420 MHz.

To minimize single-beam confusion, we required the nearest optical neighbor to be at least $\sim 2'.9$ from the target galaxy, so that only one plausible optical counterpart lies within a FAST beam. We then associated FASHI sources to SDSS targets within $\sim 2'.9$ and $|\Delta v| \leq 1000 \text{ km s}^{-1}$. To ensure a high H I detection rate (> 50%), we applied a redshift cut of $z \leq 0.03$. The mean value of H I mass in FASHI is $\sim 10^{9.4} M_{\odot}$. Following Bradford et al. (2015), galaxies with stellar mass $\log(M_*/M_\odot) \geq 9.5$ have H I masses typically have $M_{\rm HI} > 10^{9.5} M_{\odot}$, while the H_I gas fraction decreases with increasing stellar mass (Catinella et al. 2018). To avoid massive and gas-poor galaxies that would reduce the detection rate, we restrict the sample to $9.5 \leq \log(M_*/M_{\odot}) \leq 10.7$ and r-band magnitude $m_r < 16$ mag. Because red and quiescent galaxies contain little HI gas (Zuo et al. 2018; Zu 2020), we further limited our sample to blue galaxies with optical colors $g - r \le 0.6$ and $\log(SFR) > -1 M_{\odot} \text{yr}^{-1}$. The final sample contains 230 group galaxies, including 154 detected in H_I. Among these, 69 are classified as centrals (55 detected), while 161 are satellites (99 detected).

For galaxies without H I detection in FASHI catalog, we estimate upper limits following the rms map in FASHI data. For each galaxy we selected the closest FASHI source with a velocity difference $|\Delta v| \leq 1000 \text{ km s}^{-1}$. We use the rms of this source and esti-

mate the upper limit following the formula from Zhang et al. (2024):

$$S_{\rm HI} = {\rm SNR} \times \sigma_{\rm rms} \times \sqrt{W_{50} \times 6.4 \text{ km s}^{-1}} ,$$
 (1)

where 6.4 km s⁻¹ is spectral resolution of FASHI. We adopt SNR = 5 and $W_{50} = 200 \text{ km s}^{-1}$. Finally, we calculated H I mass via the formula (Meyer et al. 2004; Ellison et al. 2018):

$$\frac{M_{\rm HI}}{M_{\odot}} = \frac{2.356 \times 10^5}{1+z} (\frac{D}{\rm Mpc})^2 \frac{S_{\rm HI}}{\rm Jy \ km \ s^{-1}},\tag{2}$$

where D is the distance of source and z is source redshift. H I gas fraction is calculated using:

$$f_{\rm HI} = \frac{M_{\rm HI}}{M_*} \ , \tag{3}$$

where M_* is the stellar mass of the galaxy.

2.2. Scaling Relation of Control Sample

We selected galaxies with group richness = 1 as the parent isolated galaxy sample and applied the same optical selection criteria used for group galaxies. To avoid potential interactions between isolated galaxies, we excluded close isolated galaxies. Following Feng et al. (2019), interacting galaxies are defined by the line of sight velocity difference of $|\Delta v| \leq 500 \text{ km s}^{-1}$ and projected separation $d_{\rm p} \leq 200 \ h^{-1}{\rm kpc}$. We selected 230 control galaxies following the distribution of group galaxies, of which 140 have H I detections. We used equation 1 to 3 to calculate H I mass and gas fraction for non-detections. Figure 1 compares the basic properties of group (purple) and control (black) galaxies, showing consistent distributions in stellar mass, redshift, and g-r color.

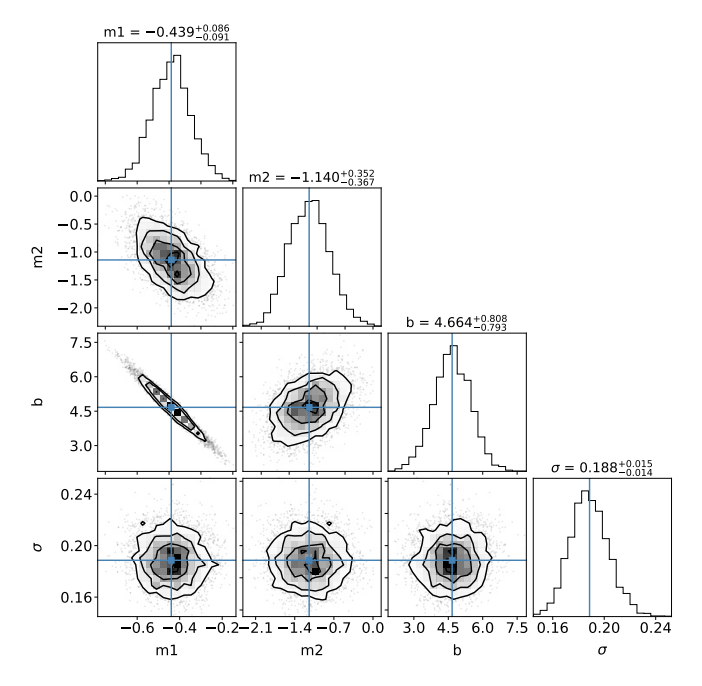


Figure 2. The posterior distributions for the H I gas fraction prediction: $\log f_{\rm HI} = m_1 \log M_* + m_2(g-r) + b + \sigma_{\rm HI}$. The blue lines show the mean values for the parameters.

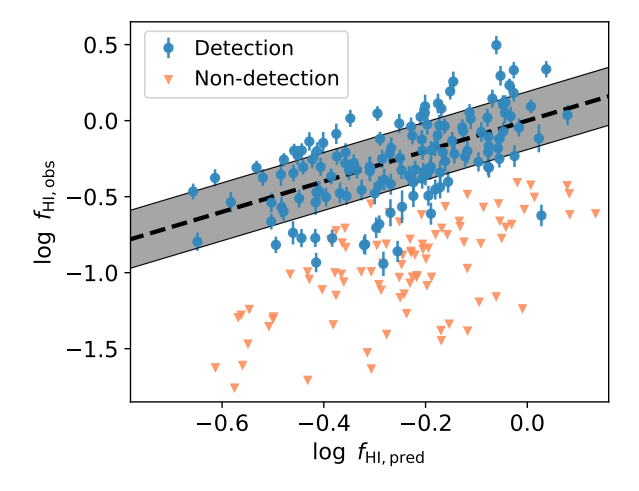


Figure 3. Predicted versus measured H I gas fraction in control galaxies. The blue points represent galaxies detected in H I, while the orange triangles indicate non-detections. The dashed line shows the one-to-one relation, and the shaded region denotes the 1σ intrinsic scatter.

To build the scaling relation for the H I gas fraction, we modeled it with a linear mixture model with stellar mass and color as:

$$\log f_{\rm HI} = m_1 \log(M_*/M_\odot) + m_2 (g-r) + b + \sigma_{\rm HI}$$
. (4)

Following Sorgho et al. (2025), we considered the Normal distribution for detections and the Censored distribution for non-detections. We use the Markov chain

Monte Carlo (MCMC) implementation to fit the relation via PyMC (Abril-Pla et al. 2023). Figure 2 shows the distributions of posteriors for H I gas fraction prediction. The fitted relation is:

$$\log f_{\rm HI} = -0.44 \log(M_*/M_{\odot}) - 1.14 (g-r) + 4.67$$
. (5)

We plot observed and predicted H_I gas fraction in Figure 3. Most of the H_I-detected galaxies (blue points) are located along the one-to-one relation (dashed line).

3. RESULTS

3.1. HI gas fraction in group galaxies

We use the Kaplan-Meier (KM) estimator to compute the median H I gas fraction for the full sample (Feigelson & Nelson 1985; Xu et al. 1998). For group galaxies, the median $\log f_{\rm HI}$ is -0.54 for the full sample and -0.27 for H I-detected galaxies. For the control galaxies, the corresponding values are -0.50 and -0.26. To compare H I gas fractions in groups with the control, we predicted the H I gas fractions in group galaxies using Equation 5. We show the observed H I gas fraction versus predicted H I gas fraction in Figure 4. The central galaxies are marked by black edges. Several satellites with H I detections lie more than 1σ below the predicted values.

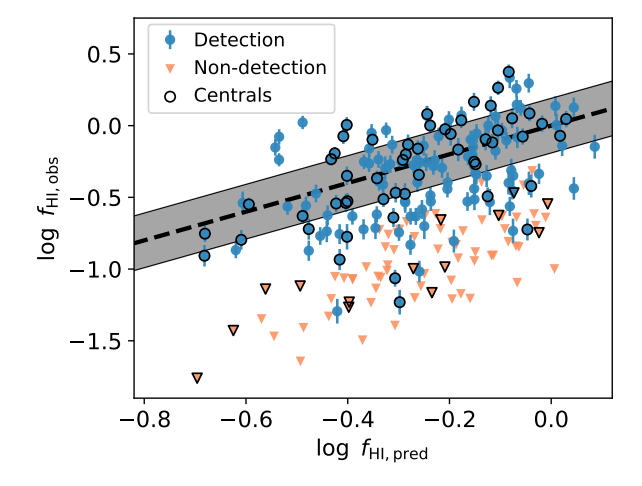


Figure 4. Predicted versus measured H_I gas fraction in group galaxies. The color scheme is the same as Figure 3. Central galaxies are marked by black edges.

We further calculated the offset of H I gas fraction $(\Delta f_{\rm HI})$ using:

$$\Delta f_{\rm HI} = \log f_{\rm HI,obs} - \log f_{\rm HI,pred}$$
 (6)

Galaxies with $\Delta f_{\rm HI} < 0$ are H I deficient than predicted by the model. Figure 5 represents the distribution of

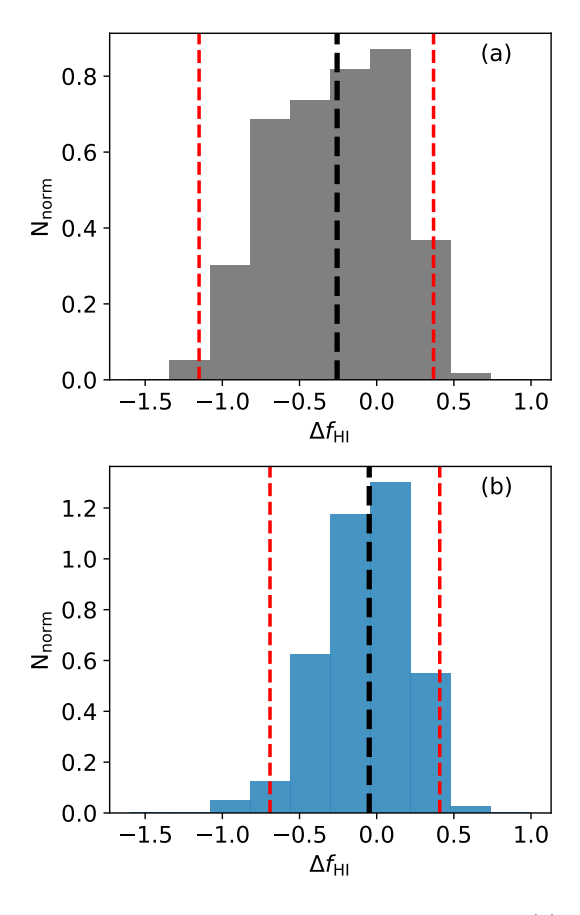


Figure 5. Distribution of $\Delta f_{\rm HI}$ in full sample (a) and H I-detections (b). The black dashed line in each panel is the median value. The region between two red dashed lines in each panel is 95% confidence interval.

 $\Delta f_{\rm HI}$ in full sample (a) and H I detections (b). Using the KM estimator, the median $\Delta f_{\rm HI}$ is -0.26 for the full sample and -0.05 for detections (Table 1). We employ a bootstrap resampling procedure to estimate the difference and 95% confidence interval between the median value of group galaxies and control ones. The difference between group and control galaxies is -0.04 in both cases. Both the H I detected and the full sample are H I deficient by $\sim 8.8\%$ compared to the control sample.

3.2. $\Delta f_{\rm HI}$ with other properties

Figure 5 and Table 1 indicate that group galaxies are H I deficient relative to both the control galaxies or the model predictions. To understand H I deficiency in group galaxies with other properties, we plot binned $\Delta f_{\rm HI}$ against stellar mass, SFR, and group richness in Figure 6(a), (b), and (c), respectively. In each violin plot, the small horizontal line marks the median value estimated using KM method. The median $\Delta f_{\rm HI}$ values

Table 1. Median Value of $\Delta f_{\rm HI}$

	Full Sample		H I-Detections	
	Median	95% C.I.	Median	95% C.I.
Group Galaxies	-0.26	[-1.15, 0.37]	-0.05	[-0.69, 0.41]
Control Galaxies	-0.21	[-1.33, 0.34]	0.002	[-0.51, 0.35]
Difference	-0.04	[-0.18, 0.16]	-0.04	[-0.14, 0.04]

of the control sample are shown as dashed lines, with blue indicating H_I-detected galaxies and black representing the full sample, respectively. Overall, more than half of group galaxies fall below the control medians.

For the full sample, the median $\Delta f_{\rm HI}$ is consistently lower than the control sample regardless of stellar mass or SFR. HI deficiency is more pronounced for the full sample with log(SFR) > 0.1 $M_{\odot} \rm yr^{-1}$ and in dense environment (richness > 10). For HI detections, Figure 6(a) and (b) show no significant dependence of $\Delta f_{\rm HI}$ on stellar mass or SFR. Figure 6(c) shows that increasing deficiency in richer groups (> 5 members). Some galaxies, particularly among the detections, still show $\Delta f_{\rm HI}$ above the control level, suggesting that group environments can lead to both gas depletion and gas enhancement.

4. DISCUSSION

4.1. Central and Satellite Galaxies

As shown in Figure 4, most satellite galaxies lie below the 1σ error region of the model unlike centrals. We calculated $\Delta f_{\rm HI}$ for central and satellite galaxies separately (Table 2). For the full sample, centrals have a median $\Delta f_{\rm HI} = -0.12$, while satellites have a median of -0.36. Compared to the control sample, the differences in $\Delta f_{\rm HI}$ are 0.13 and 0.01 for the total and H I-detected centrals, respectively, corresponding to enhancements in H I gas fraction of $\sim 35\%$ and $\sim 2.3\%$. By contrast, satellites show differences of -0.12 (full sample) and -0.06 (H I-detected), indicating H I deficiencies of $\sim 24\%$ and $\sim 13\%$, respectively. Central galaxies tend to be H I-rich, but satellite galaxies tend to be H I-poor in groups.

We plot the binned results of median $\Delta f_{\rm HI}$ of central and satellite galaxies in Figure 7. The error bars are 16-84% confidence interval calculated using the KM es-

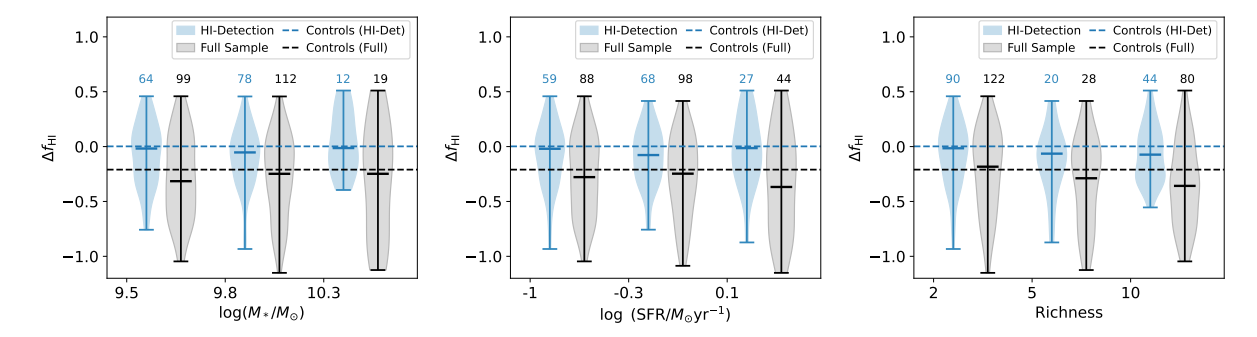


Figure 6. $\Delta f_{\rm HI}$ of group galaxies versus properties in different bins: stellar mass (a), SFR (b), group richness (c). Black and blue violins are the results of the full sample and H_I-detections, respectively. The small horizontal line in each violin region indicates the median value. The number of galaxies is indicated above the corresponding violin. The median $\Delta f_{\rm HI}$ of the control sample is shown as a blue dashed line for H_I-detections and as a black dashed line for the full sample, respectively.

timator. The central and satellite galaxies are shown using diamonds and stars, respectively. The black and blue dashed line indicates the median $\Delta f_{\rm HI}$ of the total control sample and that of the H I detected control sample. In addition to the stellar mass, SFR, and group richness, we also consider the projected distance between each satellite galaxy and the central galaxy of its host halo. For centrals, we use the distance to the nearest satellite, normalized by the group halo radius R_{180} . We calculate R_{180} via Yang et al. (2007):

$$R_{180} = 1.26 \ h^{-1} \ \text{Mpc} \left(\frac{M_h}{10^{14} h^{-1} M_{\odot}}\right)^{1/3} (1 + z_{\text{group}})^{-1} ,$$
(7)

where M_h is the halo mass adopted directly from the catalog of Yang et al. (2007). But the group halo mass is only available for massive halos with $M_h \geq 10^{11.5} M_{\odot}$. Consequently, only 171 galaxies in our sample have available halo mass estimates for their host halos. We plot binned $\Delta f_{\rm HI}$ against R/R_{180} for central and satellite galaxies in Figure 7(d).

H_I deficiency is more evident in low mass $(M_* < 10^{9.8} M_{\odot})$ satellites and in high mass $(M_* > 10^{10.3} M_{\odot})$ centrals. It is also significant in satellites with low SFR $(\log(\text{SFR}) < -0.3 \text{ M}_{\odot}\text{yr}^{-1})$ and in centrals with high SFR $(\log(\text{SFR}) > 0.1 \text{ M}_{\odot}\text{yr}^{-1})$. Among satellites, H_I detections show no clear dependence on group richness, whereas the full sample indicates a deficiency in richer environments (richness > 10). H_I deficiency becomes more pronounced as satellites approach the group center $(R/R_{180} < 0.5)$. By contrast, H_I-detected central galaxies exhibit an enhancement in H_I fraction when their nearest satellite lies beyond $0.5R/R_{180}$.

4.2. Comparison with previous studies

Several studies have investigated the H I deficiency in HCGs. Jones et al. (2023) analyzed VLA H I observa-

Table 2. Median Value of $\Delta f_{\rm HI}$ in Centrals and Satellites

$ \begin{array}{c ccccccccccccccccccccccccccccccccccc$		Full Sample		H _I -Detections	
Difference to Controls Satellites -0.36 [-1.15, 0.33] -0.07 [-0.64, 0.40] Difference -0.12 [-0.31, 0.08] -0.06 [-0.22, 0.02]		Median	95% C.I.	Median	95% C.I.
to Controls Satellites -0.36 [-1.15, 0.33] -0.07 [-0.64, 0.40] Difference -0.12 [-0.31, 0.08] -0.06 [-0.22, 0.02]	Centrals	-0.12	[-1.06, 0.37]	0.02	[-0.73, 0.39]
Satellites -0.36 [-1.15, 0.33] -0.07 [-0.64, 0.40] Difference -0.12 [-0.31, 0.08] -0.06 [-0.22, 0.02]	Difference	0.13	[-0.02, 0.33]	0.01	[-0.12, 0.10]
Difference -0.12 [-0.31, 0.08] -0.06 [-0.22, 0.02]	to Controls				
. , , , , ,	Satellites	-0.36	[-1.15, 0.33]	-0.07	[-0.64, 0.40]
to Controls	Difference	-0.12	[-0.31, 0.08]	-0.06	[-0.22, 0.02]
	$\underline{\text{to Controls}}$				

tions of 38 HCGs, and Sorgho et al. (2025) observed 6 HCGs with MeerKAT. Both studies found that HCGs generally contain less HI than predicted by scaling relations, with the deficiency being most pronounced in systems where the atomic gas is entirely removed or undetected. HCGs have low richness, typically containing 4-10 members, but they are compact with local density (Σ) above 100 gal Mpc⁻² (Hickson 1982). For comparison, we estimated the local density for our sample by selecting galaxies within $\Delta v \leq 1000 \text{ km s}^{-1}$. For each target galaxy, we identified the five nearest neighbors and measured the projected distance to the fifth neighbor (d_5) . The local density was calculated as $5/(\pi d_5^2)$. The median local density is $0.58 \text{ gal Mpc}^{-2}$ for control galaxies and 2.79 gal Mpc⁻² for group galaxies, respectively. We plot $\Delta f_{\rm HI}$ versus local density in Figure 8. H_I deficiency becomes significant at $\Sigma > 10$ gal Mpc⁻², where the H_I-detected group sample has a median $\Delta f_{\rm HI} = -0.19$, and the full sample exhibits a stronger deficiency with a median $\Delta f_{\rm HI} = -0.56$. The maximum local density in our sample is $\Sigma = 65$ gal Mpc⁻², lower than that of HCGs, yet still consistent with increasing deficiency toward denser environments. In addition,

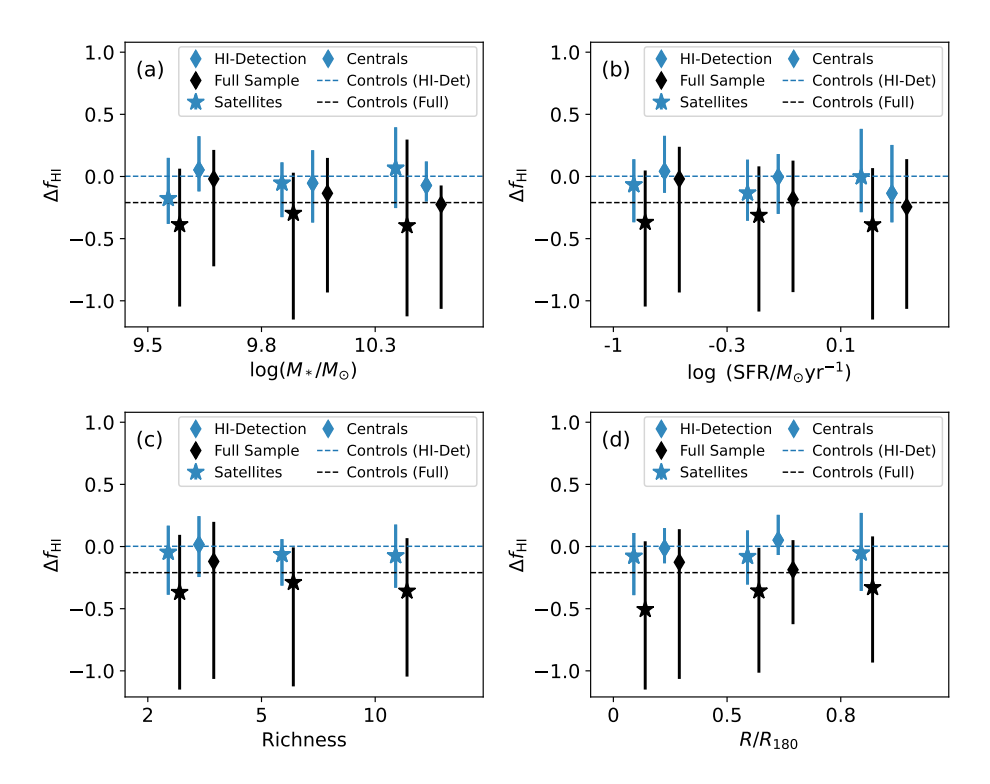


Figure 7. Median $\Delta f_{\rm HI}$ of central and satellite galaxies against stellar mass (a), SFR (b), richness (c), and R/R_{180} (d). Black and blue color indicates the results of the full sample and H I-detections, respectively. The error bars are 16% \sim 84% confidence interval. Central and satellite galaxies are shown using diamonds and stars, respectively. The median $\Delta f_{\rm HI}$ of the control sample is shown as a blue dashed line for H I detections and as a black dashed line for the full sample, respectively.

satellite galaxies with low stellar mass $(M_* < 10^{9.8} M_{\odot})$ remain significant H_I-deficient (Figure 7(a)). In low-mass systems or dense region, environmental processes such as ram pressure stripping and tidal interactions are likely to remove gas efficiently, leading to reduced atomic gas content.

Janowiecki et al. (2017) studied HI content of central galaxies using Arecibo data and found that they generally have higher HI content than isolated galaxies. They also reported that centrals with more distant nearest satellites show stronger HI enhancement. Consistent with this, Figure 7(a) shows an enhancement in low-mass central galaxies $(M_* < 10^{9.8} M_{\odot})$. Since central galaxies are typically the brightest members of their host groups, such low-mass centrals likely reside in low-mass groups. As suggested by Janowiecki et al. (2017), central galaxies in low-mass groups may have gas contributions from the cosmic web or recent H I-rich minor mergers. Wang et al. (2023) also reported that condensation of gas from the intergalactic medium can enhance the HI content of NGC 4631. Furthermore, Figure 7(d) indicates that central galaxies whose nearest satellite lies beyond $0.5R/R_{180}$ exhibit enhanced H I content, suggesting possible ongoing gas accretion.

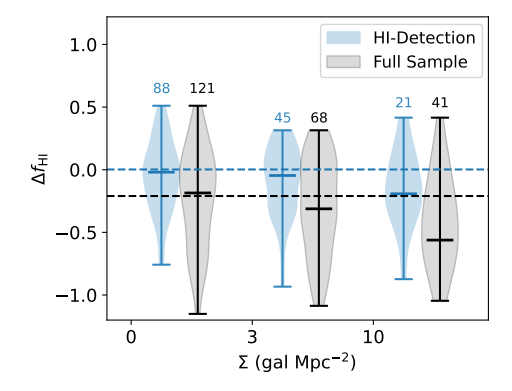


Figure 8. $\Delta f_{\rm HI}$ of group galaxies versus local density (Σ). The color schemes are same as Figure 6.

Brown et al. (2023) studied star formation in 33 Virgo Cluster satellite galaxies and found that H I-poor galaxies have a reduced SFR surface density compared to H I-normal cluster or field galaxies. Ram pressure stripping plays a key role in depleting atomic gas reservoirs and quenching star formation. Figure 7(b) demonstrates that H I detected satellite galaxies with low SFR ($\log(\text{SFR}/M_{\odot}\text{yr}^{-1}) < 0.1$) are more H I-poor. This is consistent with the scenario proposed by Jaffé et al. (2015), in which satellites lose gas as they settle into the cluster potential, leading to suppressed star for-

mation. Our results support this interpretation, as reduced atomic gas reservoirs appear directly linked to lower SFR in these galaxies.

However, Figure 7 (a) and (b) shows that central galaxies exhibit trends distinct from those of satellites. Janowiecki et al. (2017) reported $\rm H_2$ observations for 7 central galaxies with stellar masses below $10^{10} M_{\odot}$, 6 of which display higher $\rm H_2$ fractions than isolated galaxies of similar mass. These findings suggest that low-mass central galaxies may simultaneously exhibit elevated H I fractions, enhanced $\rm H_2$ content, and increased SFR. In contrast to satellites, which tend to lose H I through stripping, central galaxies may accrete cold gas from their surroundings, sustaining or even boosting their star formation activity.

5. SUMMARY

In this work, we investigated the H I content of group galaxies using FASHI data and the SDSS DR7 catalog. Our sample contains 230 group galaxies from Yang et al. (2007), including 154 H I detections. Of these, 69 are central galaxies (55 detections) and 161 are satellites (99 detections). For comparison, we constructed a control sample of 230 isolated galaxies, matched in stellar mass and color to the group galaxies. We use the control sample to establish a scaling relation between H I gas fraction and optical properties. We then applied the relation to predict the H I content of the group galaxies. The main conclusions of this study are summarized below:

- 1. We estimate the median $\Delta f_{\rm HI}$ using the KM estimator. For the full sample, the median is -0.26 (95% CI [-1.15,~0.37]), while it is -0.05 (95% CI [-0.69,~0.41]) for H_I-detected galaxies. Both the full group galaxies and H_I-detected group galaxies show mild H_I deficiency compared to the control sample. The difference of $\Delta f_{\rm HI}$ between group and control galaxies is -0.04, corresponding to an $\sim 8.8\%$ lower H_I content in group galaxies compared to isolated systems.
- 2. More than 50% of group galaxies have $\Delta f_{\rm HI}$ values below those of the control sample, independent of stellar mass, SFR, and richness. Low $\Delta f_{\rm HI}$ is more pronounced in the full sample with log(SFR) > 0.1 $M_{\odot}{\rm yr}^{-1}$ and in denser environments (richness > 10 or Σ > 10 gal Mpc⁻²).
- 3. Central and satellite galaxies exhibit distinct evolutionary trends in their H I content. The total central

galaxies have H I gas fraction $\sim 35\%$ higher than control ones. Centrals likely accrete gas from minor mergers or the cosmic web, enhancing their H I reservoirs, consistent with the findings of Janowiecki et al. (2017). In contrast, satellite galaxies tend to lose gas when entering denser regions, resulting in H I depletion. The total satellite population has an H I gas fraction $\sim 24\%$ below the controls.

In conclusion, we have investigated HI gas content of group galaxies using recent FASHI data, providing a systematic view of atomic gas evolution in galaxy groups. Group galaxies show a mild deficit in HI relative to control systems, with the deficiency becoming more significant in denser regions (richness > 10 or $\Sigma > 10 \text{ gal Mpc}^{-2}$). H I deficiency is evident in satellite galaxies, consistent with possible gas removal through ram pressure stripping. Central galaxies exhibit mildly enhanced HI content, suggesting that they may be accreting gas from their surroundings. Future observations focusing on molecular gas in group galaxies, based on our studies, will provide deeper insight into the regulation of cold gas and star formation in group environments. In addition, future X-ray observations will help characterize the hot intragroup medium, enabling a more precise assessment of halo stripping processes.

This work is supported by the National Natural Science Foundation of China under Nos. 11890692, 12133008, 12221003. We acknowledge the science research grants from the China Manned Space Project with No. CMS-CSST-2021-A04 and No. CMS-CSST-2025-A10. QY was supported by the European Research Council (ERC) under grant agreement No. 101040751. This work uses the data from FASHI project. FASHI made use of the data from FAST (Five-hundred-meter Aperture Spherical radio Telescope). FAST is a Chinese national mega-science facility, operated by National Astronomical Observatories, Chinese Academy of Sciences.

Funding for the Sloan Digital Sky Survey IV has been provided by the Alfred P. Sloan Foundation, the U.S. Department of Energy Office of Science, and the Participating Institutions. SDSS-IV acknowledges support and resources from the Center for High Performance Computing at the University of Utah. The SDSS website is www.sdss.org.

SDSS-IV is managed by the Astrophysical Research Consortium for the Participating Institutions of the SDSS Collaboration, including the Brazilian Participation Group, the Carnegie Institution for Science, Carnegie Mellon University, Harvard-Smithsonian Center for Astrophysics, the Chilean Participation Group, the French Participation Group, Instituto de Astrofísica de Canarias, The Johns Hopkins University, Kavli Institute for the Physics and Mathematics of the Universe (IPMU) / University of Tokyo, the Korean Participation Group, Lawrence Berkeley National Laboratory, Leibniz Institut für Astrophysik Potsdam (AIP), Max-Planck-Institut für Astrophysik (MPIA Heidelberg), Max-Planck-Institut für Astrophysik (MPA Garching), Max-Planck-Institut für Extraterrestrische Physik (MPE), National Astronomical Observatories of China, New Mexico State University, New York University,

University of Notre Dame, Observatário Nacional / MCTI, The Ohio State University, Pennsylvania State University, Shanghai Astronomical Observatory, United Kingdom Participation Group, Universidad Nacional Autónoma de México, University of Arizona, University of Colorado Boulder, University of Oxford, University of Portsmouth, University of Utah, University of Virginia, University of Washington, University of Wisconsin, Vanderbilt University, and Yale University.

Software: Astropy (Astropy Collaboration et al. 2013), PyMC (Abril-Pla et al. 2023), SciPy (Virtanen et al. 2020), TOPCAT (Taylor 2005).

REFERENCES

Abril-Pla, O., Andreani, V., Carroll, C., et al. 2023, PeerJ Computer Science, 9, doi: 10.7717/peerj-cs.1516

Ai, M., & Zhu, M. 2018, ApJ, 862, 48, doi: 10.3847/1538-4357/aac9b7

Astropy Collaboration, Robitaille, T. P., Tollerud, E. J., et al. 2013, A&A, 558, A33,

doi: 10.1051/0004-6361/201322068

Barnes, D. G., Staveley-Smith, L., de Blok, W. J. G., et al. 2001, MNRAS, 322, 486,

doi: 10.1046/j.1365-8711.2001.04102.x

Boselli, A., & Gavazzi, G. 2006, PASP, 118, 517, doi: 10.1086/500691

Bradford, J. D., Geha, M. C., & Blanton, M. R. 2015, ApJ, 809, 146, doi: 10.1088/0004-637X/809/2/146

Brown, T., Roberts, I. D., Thorp, M., et al. 2023, ApJ, 956, 37, doi: 10.3847/1538-4357/acf195

Catinella, B., Schiminovich, D., Kauffmann, G., et al. 2010, MNRAS, 403, 683, doi: 10.1111/j.1365-2966.2009.16180.x

Catinella, B., Saintonge, A., Janowiecki, S., et al. 2018, MNRAS, 476, 875, doi: 10.1093/mnras/sty089

Cayatte, V., Kotanyi, C., Balkowski, C., & van Gorkom, J. H. 1994, AJ, 107, 1003, doi: 10.1086/116913

Cayatte, V., van Gorkom, J. H., Balkowski, C., & Kotanyi, C. 1990, AJ, 100, 604, doi: 10.1086/115545

Chung, A., van Gorkom, J. H., Kenney, J. D. P., Crowl, H., & Vollmer, B. 2009, AJ, 138, 1741, doi: 10.1088/0004-6256/138/6/1741

Cortese, L., Catinella, B., Boissier, S., Boselli, A., & Heinis, S. 2011, MNRAS, 415, 1797, doi: 10.1111/j.1365-2966.2011.18822.x

Cortese, L., Catinella, B., & Smith, R. 2021, PASA, 38, e035, doi: 10.1017/pasa.2021.18

Deb, T., Verheijen, M. A. W., & van der Hulst, J. M. 2023, A&A, 676, A118, doi: 10.1051/0004-6361/202244910 Dénes, H., Kilborn, V. A., & Koribalski, B. S. 2014, MNRAS, 444, 667, doi: 10.1093/mnras/stu1337

Ellison, S. L., Catinella, B., & Cortese, L. 2018, MNRAS, 478, 3447, doi: 10.1093/mnras/sty1247

Feigelson, E. D., & Nelson, P. I. 1985, ApJ, 293, 192, doi: 10.1086/163225

Feng, S., Shen, S.-Y., Yuan, F.-T., et al. 2019, ApJ, 880, 114, doi: 10.3847/1538-4357/ab24da

For, B. Q., Wang, J., Westmeier, T., et al. 2021, MNRAS, 507, 2300, doi: 10.1093/mnras/stab2257

Gunn, J. E., & Gott, III, J. R. 1972, ApJ, 176, 1, doi: 10.1086/151605

Haynes, M. P., Giovanelli, R., Kent, B. R., et al. 2018, ApJ, 861, 49, doi: 10.3847/1538-4357/aac956

Hibbard, J. E., & van Gorkom, J. H. 1996, AJ, 111, 655, doi: 10.1086/117815

Hickson, P. 1982, ApJ, 255, 382, doi: 10.1086/159838

Hu, W., Cortese, L., Staveley-Smith, L., et al. 2021, MNRAS, 507, 5580, doi: 10.1093/mnras/stab2431

Huchtmeier, W. K. 1997, A&A, 325, 473

Jaffé, Y. L., Smith, R., Candlish, G. N., et al. 2015, MNRAS, 448, 1715, doi: 10.1093/mnras/stv100

Janowiecki, S., Catinella, B., Cortese, L., et al. 2017, MNRAS, 466, 4795, doi: 10.1093/mnras/stx046

Jiang, P., Yue, Y., Gan, H., et al. 2019, Science China Physics, Mechanics, and Astronomy, 62, 959502, doi: 10.1007/s11433-018-9376-1

Jiang, P., Tang, N.-Y., Hou, L.-G., et al. 2020, Research in Astronomy and Astrophysics, 20, 064, doi: 10.1088/1674-4527/20/5/64

Jones, M. G., Espada, D., Verdes-Montenegro, L., et al. 2018, A&A, 609, A17, doi: 10.1051/0004-6361/201731448

Jones, M. G., Verdes-Montenegro, L., Moldon, J., et al. 2023, A&A, 670, A21, doi: 10.1051/0004-6361/202244622

- Koribalski, B. S., Staveley-Smith, L., Westmeier, T., et al. 2020, Ap&SS, 365, 118, doi: 10.1007/s10509-020-03831-4
- Li, X., Li, C., Mo, H. J., Xiao, T., & Wang, J. 2022, ApJ, 941, 48, doi: 10.3847/1538-4357/ac9ccb
- Liu, Y., Zhu, M., Yu, H., et al. 2023, MNRAS, 523, 3905, doi: 10.1093/mnras/stad1281
- Lu, Y., Yang, X., Liu, C., et al. 2024, Science China Physics, Mechanics, and Astronomy, 67, 119511, doi: 10.1007/s11433-024-2440-3
- Luber, N. M., Hasan, F., van Gorkom, J. H., et al. 2025, ApJ, 985, 214, doi: 10.3847/1538-4357/adc448
- Meyer, M. J., Zwaan, M. A., Webster, R. L., et al. 2004, MNRAS, 350, 1195, doi: 10.1111/j.1365-2966.2004.07710.x
- Moretti, A., Paladino, R., Poggianti, B. M., et al. 2020, ApJL, 897, L30, doi: 10.3847/2041-8213/ab9f3b
- Moretti, A., Serra, P., Bacchini, C., et al. 2023, ApJ, 955, 153, doi: 10.3847/1538-4357/aceda4
- Odekon, M. C., Koopmann, R. A., Haynes, M. P., et al. 2016, ApJ, 824, 110, doi: 10.3847/0004-637X/824/2/110
- Salim, S., Lee, J. C., Janowiecki, S., et al. 2016, ApJS, 227, 2, doi: 10.3847/0067-0049/227/1/2
- Serra, P., Oosterloo, T., Morganti, R., et al. 2012, MNRAS, 422, 1835, doi: 10.1111/j.1365-2966.2012.20219.x
- Solanes, J. M., Manrique, A., García-Gómez, C., et al. 2001, ApJ, 548, 97, doi: 10.1086/318672
- Sorgho, A., Verdes-Montenegro, L., Ianjamasimanana, R., et al. 2025, A&A, 696, A177, doi: 10.1051/0004-6361/202452995
- Stark, D. V., Kannappan, S. J., Eckert, K. D., et al. 2016, ApJ, 832, 126, doi: 10.3847/0004-637X/832/2/126

- Taylor, M. B. 2005, in Astronomical Society of the Pacific Conference Series, Vol. 347, Astronomical Data Analysis Software and Systems XIV, ed. P. Shopbell, M. Britton, & R. Ebert, 29
- Verdes-Montenegro, L., Yun, M. S., Williams, B. A., et al. 2001, A&A, 377, 812, doi: 10.1051/0004-6361:20011127
- Virtanen, P., Gommers, R., Oliphant, T. E., et al. 2020, Nature Methods, 17, 261, doi: 10.1038/s41592-019-0686-2
- Vollmer, B., Cayatte, V., Balkowski, C., & Duschl, W. J. 2001, ApJ, 561, 708, doi: 10.1086/323368
- Wang, J., Yang, D., Oh, S. H., et al. 2023, ApJ, 944, 102, doi: 10.3847/1538-4357/acafe8
- Williams, B. A., Yun, M. S., & Verdes-Montenegro, L. 2002, AJ, 123, 2417, doi: 10.1086/339839
- Xu, C., Hacking, P. B., Fang, F., et al. 1998, ApJ, 508, 576, doi: 10.1086/306424
- Xu, J.-L., Zhu, M., Yu, N., et al. 2023, ApJL, 944, L40, doi: 10.3847/2041-8213/acb932
- Yang, X., Mo, H. J., van den Bosch, F. C., & Jing, Y. P. 2005, MNRAS, 356, 1293, doi: 10.1111/j.1365-2966.2005.08560.x
- Yang, X., Mo, H. J., van den Bosch, F. C., et al. 2007, ApJ, 671, 153, doi: 10.1086/522027
- Yu, H., Zhu, M., Xu, J.-L., et al. 2023, MNRAS, 521, 2719, doi: 10.1093/mnras/stad436
- Zabel, N., Brown, T., Wilson, C. D., et al. 2022, ApJ, 933, 10, doi: 10.3847/1538-4357/ac6e68
- Zhang, C.-P., Zhu, M., Jiang, P., et al. 2024, Science China Physics, Mechanics, and Astronomy, 67, 219511, doi: 10.1007/s11433-023-2219-7
- Zhou, R., Zhu, M., Yang, Y., et al. 2023, ApJ, 952, 130, doi: 10.3847/1538-4357/acdcf5
- Zhu, M., Yu, H., Wang, J., et al. 2021, ApJL, 922, L21, doi: 10.3847/2041-8213/ac350a
- Zu, Y. 2020, MNRAS, 496, 111, doi: 10.1093/mnras/staa1457
- Zuo, P., Xu, C. K., Yun, M. S., et al. 2018, ApJS, 237, 2, doi: 10.3847/1538-4365/aabd30